Lava lake level as a gauge of magma reservoir pressure and eruptive hazard

Matthew R. Patrick, Kyle R. Anderson, Michael P. Poland, Tim R. Orr, and Donald A. Swanson
U.S. Geological Survey – Hawaiian Volcano Observatory

Additional Methods

1.1 Monitoring network

Figure DR1 shows the position of the lava lake relative to summit GPS and tilt instruments, as well as the cameras used for monitoring lava lake level. GPS processing is described in Miklius et al. (2005).

1.2 Lava level measurements

The majority of data points in the lava level time series (February 2011-June 2014) were derived from hourly images collected by the HTcam thermal camera on the rim of Halemaʻumaʻu Crater (Fig. 1, DR1). The HTcam thermal camera is a Mikron M7500 longwave (7.5-13 microns) camera with an image size of 320 x 240 pixels, having a horizontal field of view of approximately 53° (Patrick et al., 2014). Lava height in image pixels was measured by hand and converted to vertical elevation using a linear fit to sporadic laser rangefinder and LIDAR measurements, and structure-from-motion (SfM) models of the vent geometry (Fig. DR2). The vent crater geometry has evolved due to rim collapses, and we divide the time period into relatively stable epochs which are separated by short periods (on the order of several days) of vent instability. Individual linear regressions were applied to each stable epoch to determine best fit coefficients linking image pixel values to laser rangefinder and LIDAR calibration points, with interpolated values used in the brief periods between these stable epochs. The resulting calibrated lava level measurements from the HTcam images have a root-mean-square residual value of 1.7 m from the calibration points. Most calibration points consist of laser rangefinder measurements of lake level taken from the Halemaʻumaʻu Overlook, in which the measurement error is about one meter. Seventeen calibration measurements were from tripod LIDAR measurements of lake level. Five calibration measurements, which are the majority of points in the later portion of 2011, are from structure-from-motion surface models of the vent. The SfM models were constructed using Agisoft Photoscan software using images collected by a handheld thermal camera during helicopter overflights of the vent. The thermal camera used for this purpose was a FLIR Systems SC620 camera with an image size of 640 x 480 pixels. About six waypoints were used to scale and geo-register each surface model, using points taken from an orthorectified WorldView 2 image of Kīlauea's summit. The error in these SfM measurements is up to a few meters.

For lava level from mid-2010 to February 2011, measurements were made from images collected from a low-light camera (HMcam) also operating on the rim of Halemaʻumaʻu Crater (Fig. DR1). These measurements were made once per day, and show the "baseline" lava level (i.e. we excluded images collected during abrupt spikes in lava level due to gas pistoning). The lava level was estimated from these image pixel values using the known field of view of the camera along with a crater geometry taken from tripod LIDAR data collected the previous year. Calibration points during this earlier period (pre-2011) were generally sparse because the crater was narrow and filled with thick fume, and the lava level was lower, making laser rangefinder and conventional theodolite measurements impossible. To check the accuracy of the image-based measurements during this period, we constructed several SfM models of the crater geometry, again using thermal images collected during helicopter overflights. The thermal camera was effective at "seeing" through the thick fume in the crater. SfM results were within five meters of the image-based estimates, confirming that they are reasonable.

In addition, lava level was measured at a finer time increment over limited periods for specific analyses. Lava level was measured from HTcam images as described above for January and February 2012, but at five-minute spacing to examine time delays with summit tilt. During November and December 2010, lava level was measured in a similar manner from HTcam images at 10-minute increments to study gas piston behavior. These 2010 measurements were done when the HTcam camera had a narrower field-of-view lens (21° horizontal field of view), and image pixels were converted to absolute elevation using a combination of the camera viewing geometry and the measured lake and crater geometry inferred from a SfM surface map (described above) constructed from helicopter thermal images collected on December 2, 2010.

1.3. Measuring area of active breakouts with webcam imagery

Images were recorded by a Stardot Netcam SC 5-megapixel camera with an 80° horizontal field of view operating in a near-infrared mode during the night hours. Nightly composite images show the maximum brightness detected in a given pixel location throughout the night (Patrick et al. 2010a). A mask was applied to eliminate areas not on the active flow field, and pixels above a 94% gray value were counted for each night. The areas of active lava were ~800 m to 3.3 km from the camera (Fig. DR3), so a simple linear distance correction was applied to the image pixels, based on image row, to correct for the variable viewing distance and estimate pixel footprint size.

The webcam was perched on high ground above the coastal plain during our study period (mid-April to mid-June, 2012) and captured activity on the lower portion of the East Rift Zone (ERZ) flow field. Two main areas of breakouts were active during this period, with the camera capturing the lowermost, which normally accounted for half, or more, of the total area of breakouts (Fig. DR3). Both areas of breakouts were fed by the same master lava tube, and therefore likely exhibited shared fluctuations in activity. Because of this, we expect that the trend shown in Figure 3C is likely a reliable depiction of fluctuations on the entire flow field.

1.4 Moving-window correlation of tilt and lava level

We used a one-week moving window, with 75% overlap, between September 2011 and June 2014, to measure the relationship between UWE radial ground tilt and lava level. Because our focus was on steady-state behavior we used data after September 2011 as they were not affected by large-scale disruptions of the magmatic system, such as ERZ eruptive events (Fig. 2D). We applied linear regression to each window period and only calculated the slope and coefficient of determination (r^2) for those windows that had tilt ranges greater than 2 microradians. The r^2 values for these results are shown in Figure DR4. To measure the slope of this linear fit, we limited these results further, to those with r^2 values >0.90 (Fig. DR5)

1.5 Cross-correlation of tilt and lava lake level

Cross-correlation of UWE radial tilt and lava level was accomplished using lava level data that were measured at approximately five-minute intervals during January and February 2012. Tilt data are sampled at one minute intervals. We performed a linear interpolation of both lava level and tilt data to a time vector with uniform five minute sampling. The cross-correlation of these data was performed with MATLAB's xcorr function (Fig. DR6).

1.6 Bulk density of lava column

The bulk density of the lava column is bracketed by two end-members possibilities: 1000 and 2500 kg m^{-3}. The maximum density is limited to that of gas-free liquid tholeiitic basalt (roughly 2600 kg m^{-3}) (Murase and McBirney, 1973), and perhaps representative of magma deeper in the magma column, below the exsolution depth of H_2O and SO_2. However, recent gravity data suggest that the Halema'uma'u lava lake and shallow magma column (upper 150 m) have a very low density, of 950 ±300 kg m^{-3} (Carbone et al., 2013). The low density suggests that large volumes of gas remain stored in the lake. Tephra ejected from the lake have bulk densities (500-2000 kg m^{-3}) (Carey et al., 2012) consistent with this low value; however, it is unclear how deep this very low bulk density region extends into the deeper system.

1.7 Derivation of the magma flux formula

We assume that volumetric flux rate Q of magma from the summit to the ERZ is linearly proportional to the difference in pressure Δp between the summit magma reservoir and the ERZ eruptive vent, resisted by the weight of magma in the ERZ conduit:

$$Q = K(\Delta p - \rho_2 g h_2) \tag{2}$$

Here K is a constant of proportionality, ρ_2 is the average magma density in the ERZ conduit, g is gravity, and h_2 is the positive vertical distance between the ERZ eruptive vent and the reservoir (Fig. DR9). Note that this model cannot account for an observed time lag of several hours between pressure changes at the summit and then at Pu'u 'Ō'ō, but we believe that it should be correct to first order once these pressure changes fully propagate through the system.

Assuming negligible atmospheric pressure so $\Delta p = p$, where p is reservoir pressure,

$$Q = K(p - \rho_2 g h_2) \tag{3}$$

Magma reaches the surface in (at least) two locations: the summit lava lake and the ERZ vent at Puʻu ʻŌʻō. The summit lava lake is in magmastatic equilibrium with the magma chamber, while the ERZ vent is not, generally, due to viscous drag in the ERZ conduit. Magmastatic equilibrium in the summit lava lake and conduit can be used to constrain reservoir pressure using $p=\rho_1 g\, h_1$, so

$$Q = Kg(\rho_1 h_1 - \rho_2 h_2) \tag{4}$$

If magma density is constant throughout the system ($\rho_1=\rho_2$) then during times of zero flux (magmastatic equilibrium in both the summit and ERZ) the elevation of the summit lava lake should be no higher than the ERZ eruptive vent. However, during brief eruptive pauses it has been observed that the surface height of the summit lava lake maintains a level roughly 80 m higher than that of the ERZ vent. This height difference suggests that the magma in the ERZ conduit is more dense than magma in the summit lava lake, consistent with observed degassing of magma at the summit and the low density of the summit lava lake (Carbone et al., 2013).

During times of zero flux, $\rho_1 h_1 = \rho_2 h_2$. Rough constraint on ρ_1 is available (Carbone et al., 2013) but ρ_2 is largely unknown. Solving for ρ_2,

$$\rho_2 = \frac{h_1|_{Q=0}}{h_2|_{Q=0}} \rho_1 \tag{5}$$

where $|_{Q=0}$ denotes the value during the zero-flux condition. Substituting into equation (4),

$$Q = Kg\rho_1\big(h_1 - h_1|_{Q=0}\big) \tag{6}$$
$$= K_c \Delta h \tag{7}$$

where Δh is the difference between summit lava lake height and its height at magmastatic equilibrium, and we have used $h_2 = h_2|_{Q=0}$ which is valid during times of constant ERZ vent height. Note that this expression is independent of absolute reservoir depth.

Finally, the time-averaged version of equation (7) is given by

$$\bar{Q} = K_c \overline{\Delta h} \tag{8}$$

Given time-averaged flux rate and height difference it is thus possible constrain K_c. We use data from April-June 2012, during which time accurate estimates of time-averaged flux rates are available (Poland, 2014), and we compute $\overline{\Delta h}$ from the lava lake time series and an observed magmastatic equilibrium elevation of approximately 922 m. Once K_c is constrained, it can be applied to the equations above for those instances when Q is not known, to translate instantaneous lava level height to instantaneous ERZ flux Q (assuming no major changes in the ERZ conduit or shallow reservoir at Puʻu ʻŌʻō).

1.8 Density difference between summit and ERZ magmas

Figure 3a shows that during mid-2012 the magmastatic equilibrium level at the summit was roughly 922 m elevation, or 80 m above that of the ERZ vent. As the magmastatic equilibrium level occurs at times of ERZ pauses when there was likely little to no flow from the summit to Puʻu ʻŌʻō, dynamic effects due to viscosity or conduit geometry cannot account for this height difference. Instead, this 80 m height difference might be explained by density differences in the magma columns. Presumably, much of this density difference is driven by different gas content. We can balance the pressure of the summit and ERZ magma columns using equation (5). We use $h_1 = h_2 + 80$, assume that the ERZ conduit and summit are connected at a depth no shallower than the Halemaʻumaʻu reservoir at 1.5 km depth (Anderson et al. 2015), and for the summit conduit use a range of bulk densities from 1000 to 2500 kg m^{-3} (section 1.6). We estimate that magma density along the ERZ is 50-130 kg m^{-3} higher than that at the summit, which is a relatively minor difference.

1.9 Correlation of modeled and observed ERZ flow field activity

Figure 3 shows a comparison of modeled ERZ effusion rates (Figure 3B) with an observed proxy for ERZ effusion rate (Fig. 3C). The latter is based on areas of active lava observed in nightly webcam images. The Figure 3 caption indicates that values for r^2 were 0.31-0.51. This range is based on using different delay times between summit and ERZ flow field activity, which Orr et al. (2014) measured as 23.9±6.4 h. To perform the comparison, we assumed that the observed ERZ effusion rate proxy based on composite images depicted nighttime activity (20:00 to 06:00), and then subtracted the time delays. The average value of the modeled ERZ effusion rate was calculated for this delay-corrected time interval, and used to perform the linear regression.

Additional References

Carey, R.J., Manga, M., Degruyter, W., Gonnerman, H., Swanson, D., Houghton, B., Orr, T., Patrick, M., 2013, Convection in a volcanic conduit recorded by bubbles: Geology, v. 41, p. 395-398

Miklius, A., Cervelli, P., Sako, M., Lisowski, M., Owen, S., Segal, P., Foster, J., Kamibayashi, K., Brooks, B., 2005, Global Positioning System Measurements on the Island of Hawaiʻi; 1997 through 2004: U.S. Geological Survey Open-File Report 2005–1425, 48 p.

Murase, T., McBirney, A.R., 1973, Properties of some common igneous rocks and their melts at high temperatures: Geological Society of America Bulletin, v. 84, p. 3563-3592.

Patrick, M., Orr, T., Sutton, A.J., Lev, E., Fee, D., 2014b, Episodic outgassing and lava level fluctuations at Kilauea Volcano's summit lava lake in Halemaʻumaʻu Crater. American Geophysical Fall Meeting abstract V33E-08.

Supplemental Figures
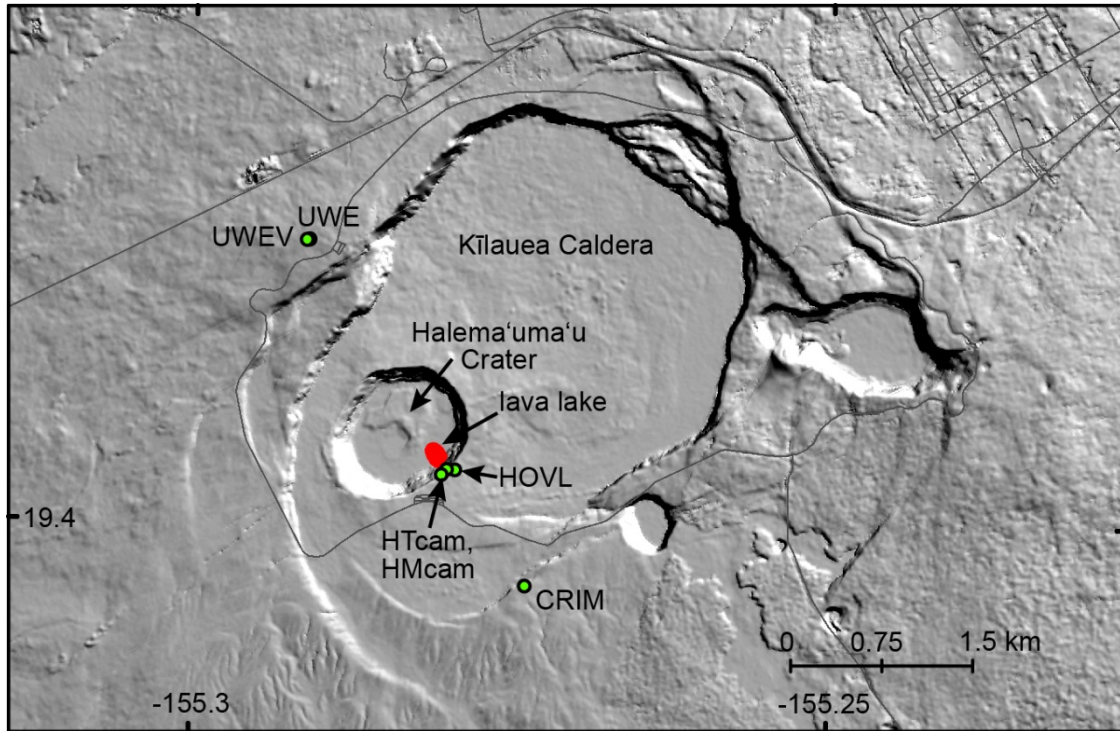
Figure DR1. Map of Kīlauea Volcano's summit region, including relevant monitoring instruments. UWEV, HOVL and CRIM are GPS instruments, and UWE measures ground tilt. HTcam is a thermal camera and HMcam is a visual-wavelength camera. Gray lines are roads.
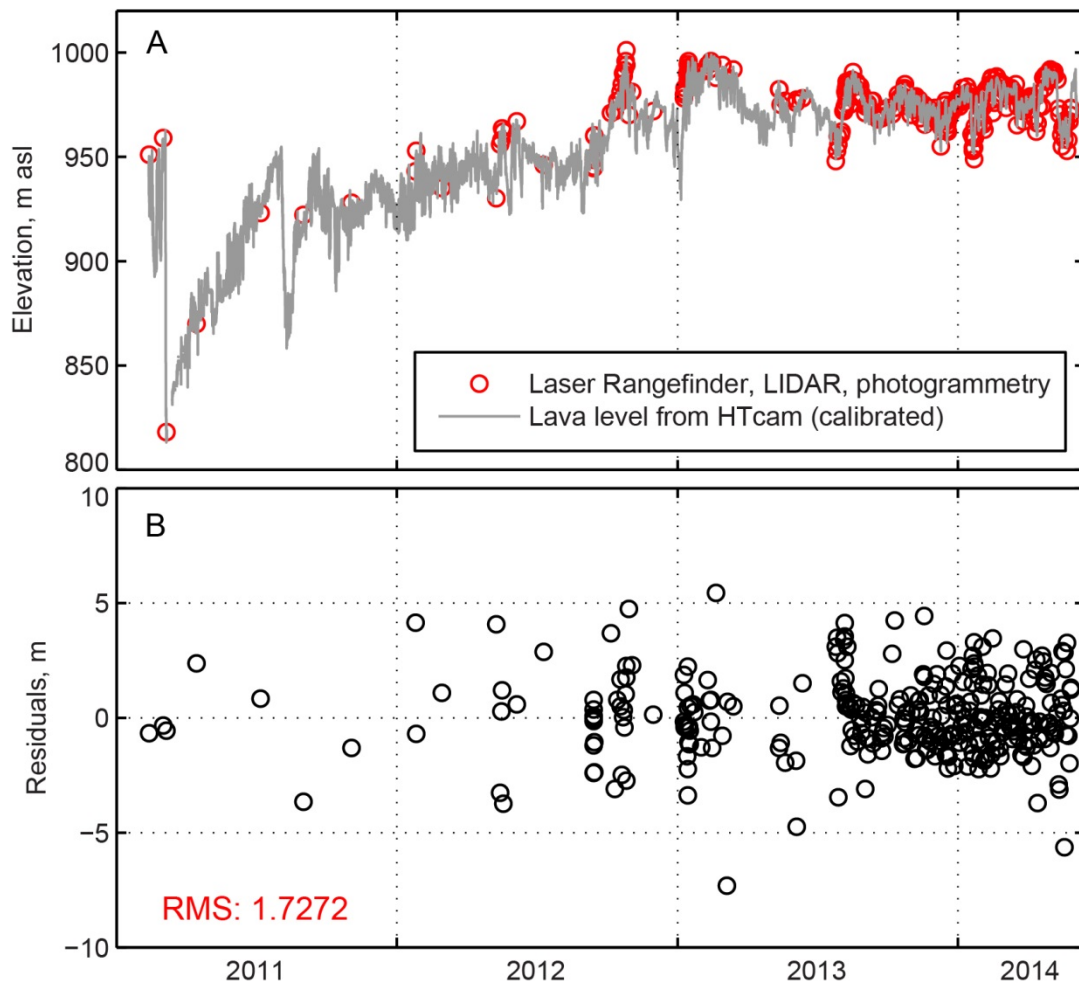
Figure DR2. Results for conversion of continuous lava level measurements from HTcam (thermal camera) images (in pixels) to elevation using sporadic calibration points from laser rangefinder (most of the points in 2013 and 2014), LIDAR, and photogrammetry measurements.
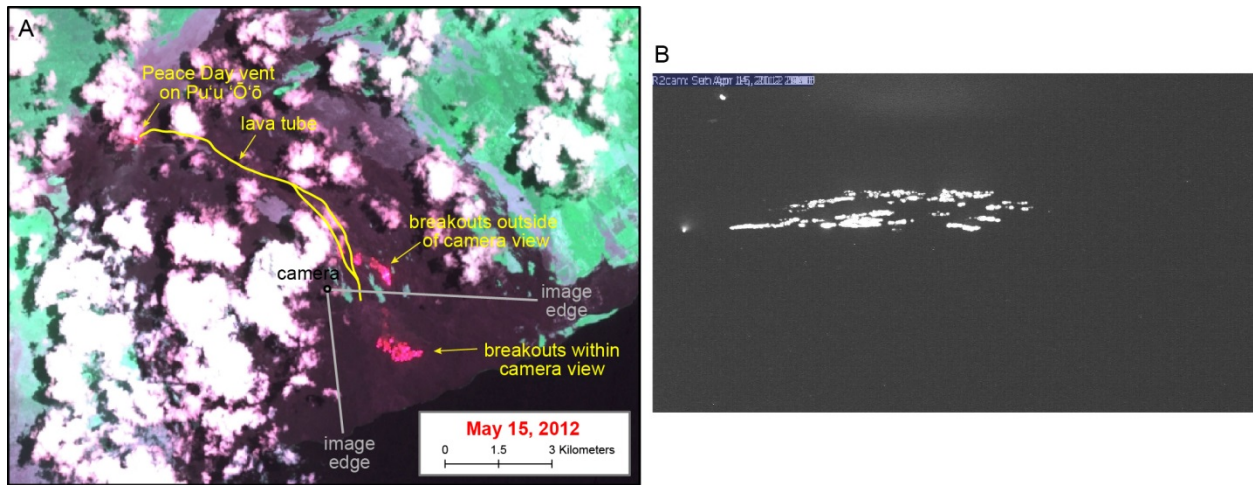
Figure DR3. Tracking activity levels on the ERZ flow field with a webcam. A. Earth Observing 1 Advanced Land Imager (EO-1 ALI) image (Bands 10-8-9 RGB) of the flow field activity on May 15, 2012. At this time two main areas of breakouts were active, with the webcam capturing the activity on the coastal plain. In general during this study period (mid-April to mid-June, 2012), the camera captured half or more of the activity. B. Sample composite image from the webcam, showing activity on the night of April 14-15, 2012. White pixels are active breakouts.
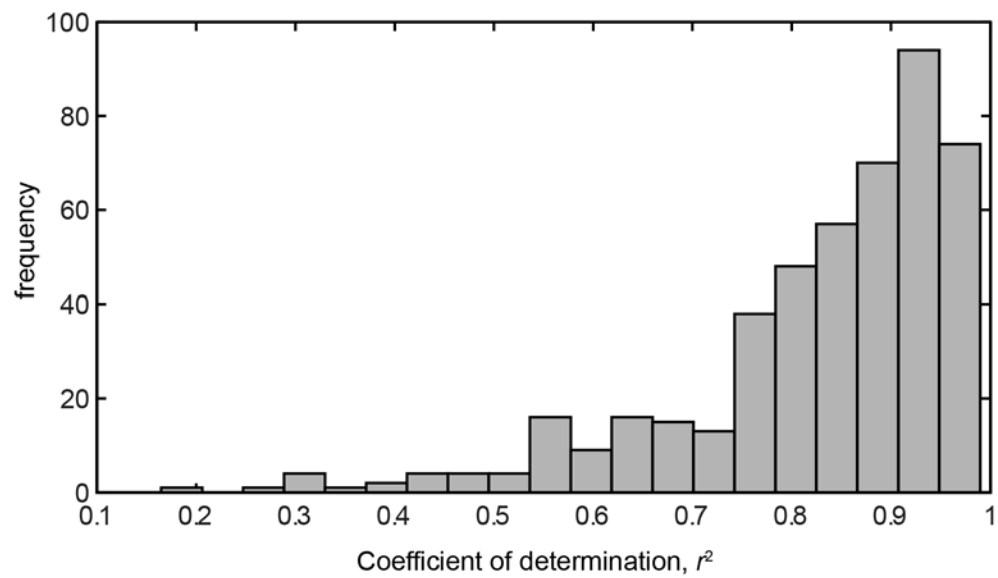
Figure DR4. One-week moving-window linear regression results, relating lava level and radial ground tilt at UWE. In most cases, the linear fits are strong and have very high r^2 values, with a mean of 0.82.
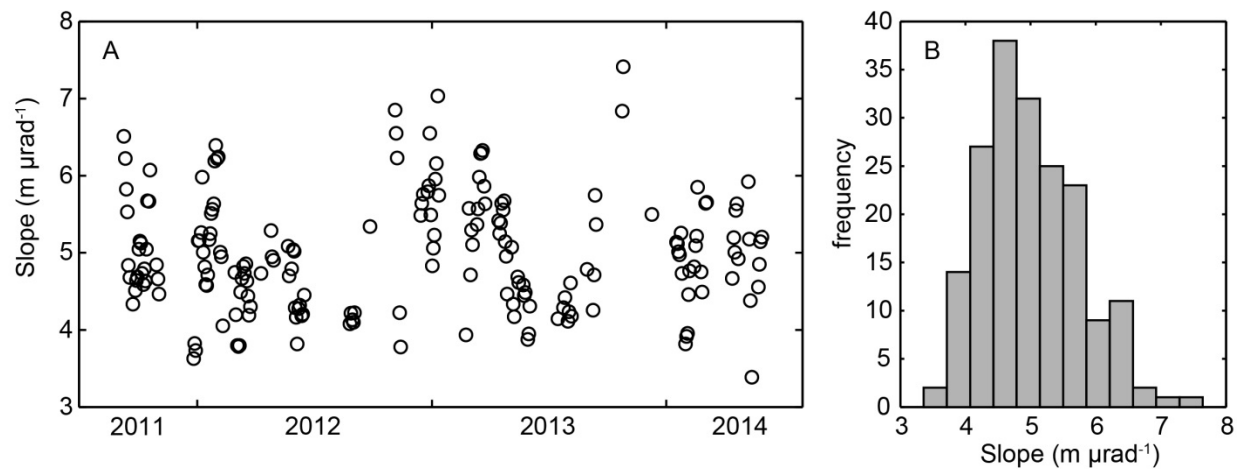
Figure DR5. One-week moving-window correlation results, showing the slope (m µrad^{-1}) of the linear regression relating lava level change and radial ground tilt at UWE, limited to those sets with $r^2>0.90$.
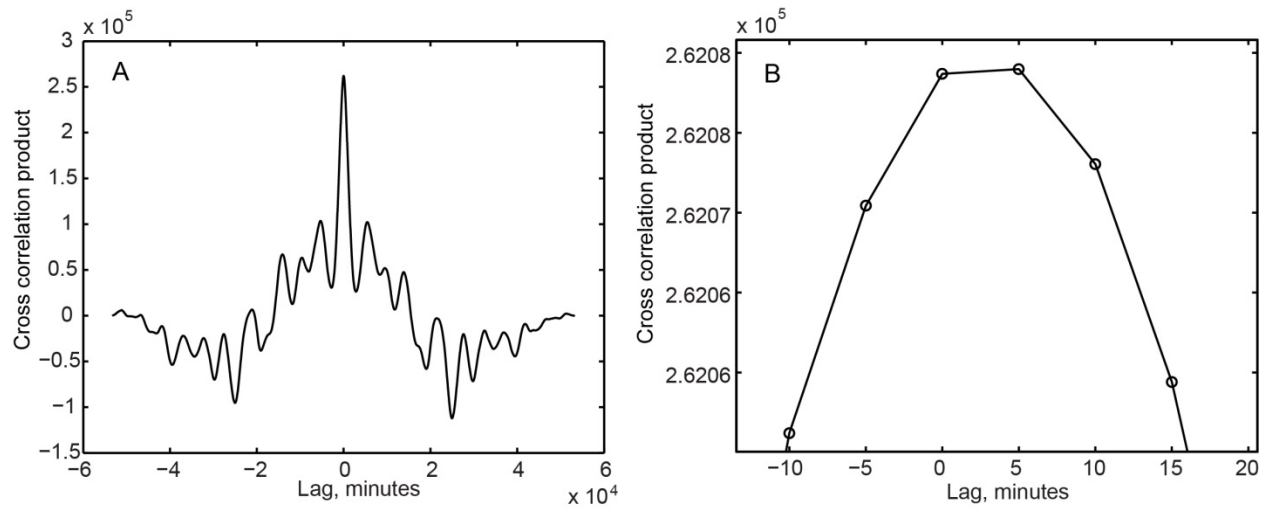
Figure DR6. Cross-correlation results for lava level and ground tilt, based on a five minute sampling interval. The peak cross-correlation product is at the five-minute lag position (i.e. lava level follows tilt by five minutes), however, the shape of the curve suggests that the actual peak resides at a lag shorter than five minutes. The precise time lag is not crucial to this study, and our results show that if a time lag does exist it is very short (several minutes) and that the lava level is responsive over short timescales to changes in magma reservoir pressure.
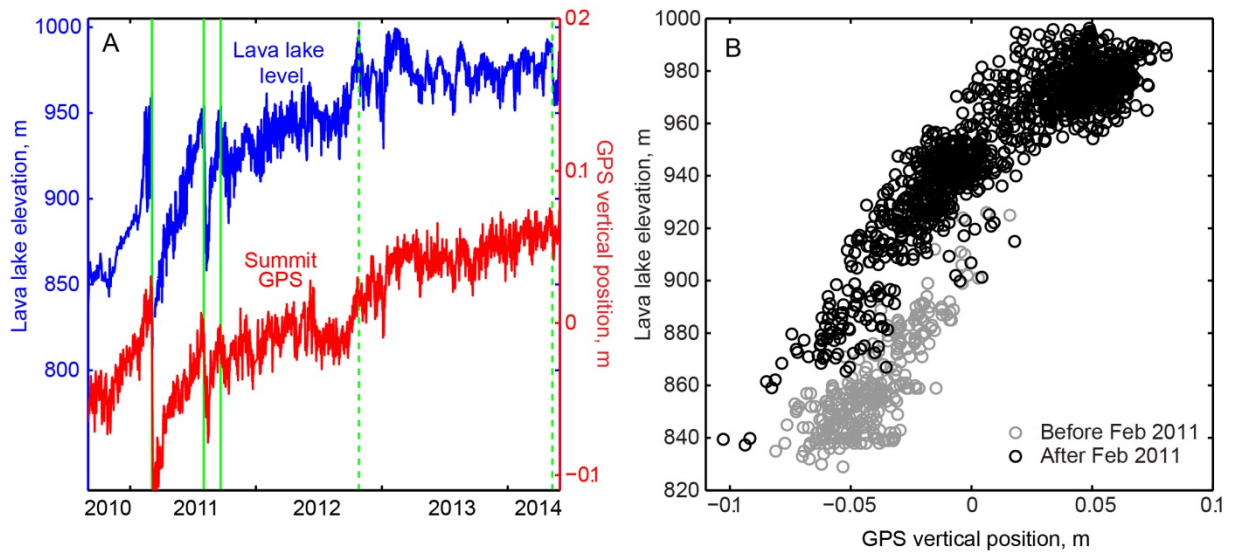
Figure DR7. Comparison of lava level and summit GPS data (vertical component at HOVL station). The scatter plot shows a roughly linear relationship. Lava level data before and after February 2011 were measured in a different manner and are shown by separate colors. Prior to February 2011, lava level was measured once a day for the baseline (non-gas-piston) level, while after February 2011 the level was measured hourly. For those data after February 2011, the average daily lava level is matched to the daily GPS solution. Vertical green lines show ERZ eruptive (solid line) and intrusive (dotted line) events. Lava lake level can be used to determine the time-varying magnitude of persistent eruptive activity on the ERZ, but it can also be useful in forecasting abrupt interruptions to this behavior. This figure shows that lava level rose to unusually high levels prior to the three eruptive events in 2011 on the ERZ. This suggests that rising magmatic pressure, tracked by GPS and lava level, reached critical levels which triggered magma to intrude from its existing ERZ conduit to create new vents.   Although the data from 2011 suggest a similar pressure threshold for these events, and would be described as "inflation predictable" (Segall, 2013), later intrusive events in 2012-2014 occurred at higher lava levels, which suggests a dynamic threshold.
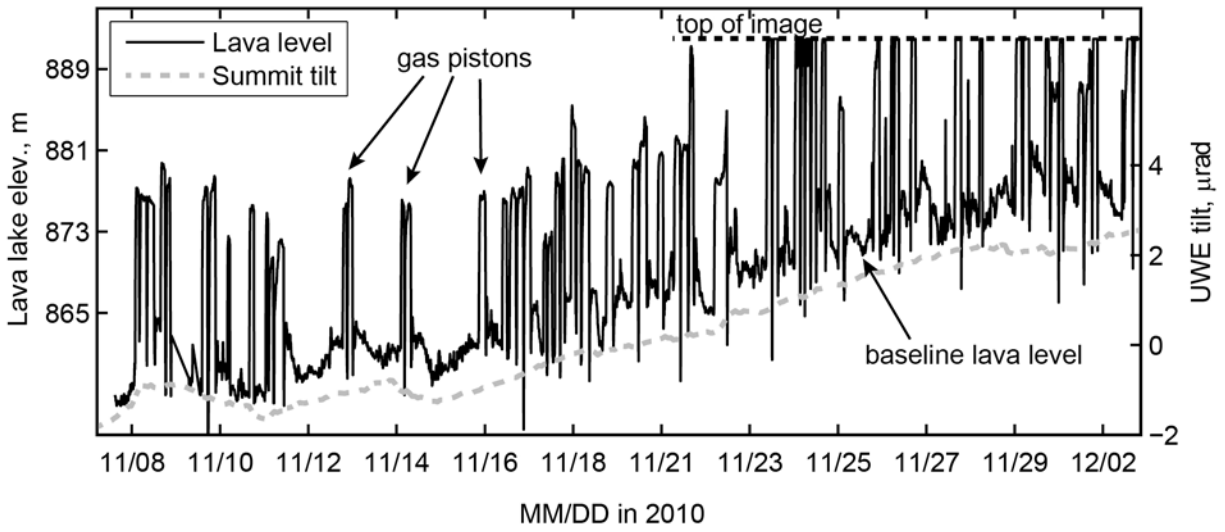
Figure DR8. Lava lake level changes due to "gas pistoning". Gas piston events can last for several hours and involve the lava level abruptly rising above its normal baseline level. Gas piston events occur sporadically (commonly a few per day during 2010-2014) and can have amplitudes of up to 20 m (Patrick et al., 2014, 2014b). They represent relatively abrupt spikes in lava level, and are relatively easy to distinguish from the gradual lava level changes that correlate with deformation data. Gas piston events can also be distinguished based on seismic tremor, as tremor drops to very low levels during the high lava stands of gas pistons. The low tremor levels are associated with a cessation of spattering at the lava lake surface due to gas accumulating in the shallow portions of the lake. The lava level was measured every 10 minutes as described in section 1.2.
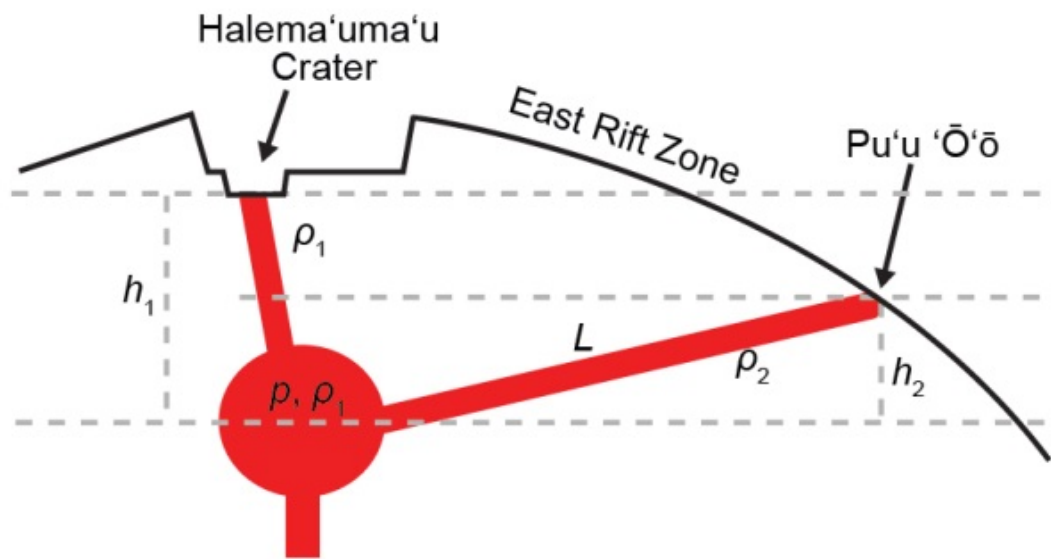
Figure DR9. Cartoon of the model geometry.